JOURNAL OF MATERIALS SCIENCE 15 (1980) 2803–2810

Characterization of Al–Si-alloys rapidly quenched from the melt

A. BENDIJK, R. DELHEZ, L. KATGERMAN, TH. H. DE KEIJSER, E. J. MITTEMEIJER, N. M. VAN DER PERS
Delft University of Technology, Laboratory of Metallurgy, Rotterdamseweg 137, 2628 AL Delft, The Netherlands

Aluminium–silicon alloys with compositions in the range 0 at % to 33.9 at % Si were rapidly quenched from the melt at cooling rates between 10^6 and 10^7 K sec^{-1} using the melt-spinning technique. The resulting ribbons were investigated by scanning electron microscopy (SEM), transmission electron microscopy (TEM), differential scanning calorimetry (DSC) and X-ray diffraction methods. Metastable solid solubilities of silicon in aluminium were determined from lattice parameter and DSC data. The values found were strongly dependent on specimen thickness and a maximum of about 5 at % Si was reached for an alloy composition of 15 at % SI (maximal equilibrium solid solubility of silicon in aluminium is 1.58 at % Si). Discrepancies between published values of metastable silicon solid solubities were related to the interpretation of the lattice parameter data. Alloy composition was shown to determine the lattice parameter of the silicon-rich phase. The crystallite sizes and the lattice distortions in the aluminium-rich and silicon-rich phases were determined by X-ray diffraction line profile analysis. From the aluminium-rich phase only strain broadening was observed whereas the silicon-rich phase gave rise to both size and strain broadening. The origin of the lattice strains was discussed. Changes in solidification behaviour are reflected in the structure parameters measured.

1. Introduction

The aluminium–silicon phase diagram consists of a simple eutectic at 12.5 at % Si and 850 K. The maximal equilibrium solid solubility of silicon in aluminium is 1.58 at % at the eutectic temperature [1]. By rapid quenching of the melt the maximum equilibrium solid solubility can be exceeded.

It is the purpose of this paper to characterize rapidly quenched Al–Si-alloys. Data are presented on the metastable solid solubility of silicon in aluminium as derived from lattice parameter measurements by X-ray diffraction methods and from results of differential scanning calorimetry (DSC). Results obtained in this study are compared with those reported in the literature (Section 3.2.). In additon, the solidification structure as identified by scanning electron microscopy (SEM), transmission electron microscopy (TEM) and X-ray diffraction line profile analysis (determination of crystallite size and microstrain) is discussed (Sections 3.1. and 3.3.).

2. Experimental procedure

2.1. Specimen preparation

Aluminium–silicon alloys with compositions in the range 0 at % to 33.9 at % Si were prepared from 99.998 wt % Al and 99.99 wt % Si. Specimens in the form of ribbons were made by melt-spinning [2]. In this technique a stream of the molten alloy, with a temperature of 120 K above the liquidus temperature, was ejected by pressurized argon from an 0.8 mm diameter orifice in the bottom of a crucible onto a polished 294 mm diameter copper wheel rotating at 3000 rpm. The metal stream coming from the orifice located 8 mm above the surface of the wheel was protected by nitrogen gas and pointed towards the axis of the wheel. The ribbons were irregular, varying in thickness from about 0.1 μm to 150 μm, and had cooling rates of 10^6 to 10^7 K sec^{-1}, according to dendrite arm spacing measurements made on TEM- and SEM-micrographs. (Compare with results in [3, 4].)

0022–2461/80/112803–06$02.60/0

2.2. Transmission and scanning electron microscopy

All the ribbons contained electron transparent areas, which could be examined in the Philips EM 300 transmission electron microscope operating at 100 kV.

A Jeol JXA-50A scanning electron microscope, operating at 10 kV, was used to examine the "wheel-side" of the ribbons after etching in Keller and Wilcox's reagent.

2.3. X-ray diffraction

2.3.1. Debije–Scherrer photographs

From each ribbon a section was cut of width 0.3 mm and length 5 mm for use as specimen in a Debije–Scherrer camera (diameter 114.7 mm, collimator diameter 0.5 mm). Diffraction patterns were obtained using Fe filtered CoKα radiation (with the tube operating at 45 kV and 24 mA, with an exposure time of 3 to 4 h). Lattice parameters of the aluminium-rich and silicon-rich phases were determined according to the Nelson–Riley extrapolation procedure [5]. In a few cases only the (4 2 0) reflection of the aluminium-rich and the (5 3 1) reflection of the silicon-rich phase were utilized.

2.3.2. Diffractometry

Each specimen for the diffractometer was composed of a number of ribbons from the melt-spun alloy placed parallel to each other. Line profiles from the aluminium-rich and silicon-rich phases were recorded using CoKα radiation. The broadening due to the instrumental aberrations and the X-ray spectrum used was eliminated with the aid of line profiles recorded from a thin silicon standard specimen (preparation described in [6]). For analysis of the profiles of the aluminium-rich phase an interpolation was performed on the 2θ-scale between the breadths of the reflections of this silicon standard.

Line profiles were recorded using a Siemens type F ω-diffractometer, with a graphite monochromator in the diffracted beam, operating at low scanning speed to obtain sufficient counting accuracy. Large portions of the background at both sides of the peaks were recorded. The background was interpolated linearly between the two extremities. For the elimination of the α_2-component [7] the ratio R (where $R = I_{\alpha_2}(\max)/I_{\alpha_1}(\max)$ and I_{α_1} and I_{α_2} are the intensities of the α_1- and α_2-components, respectively) was taken from a high angle reflection of the standard specimen.

2.4. Differential scanning calorimetry

Samples of weight approximately 8 mg were heated in closed aluminium pans in a Du Pont differential scanning calorimeter (model 990 with a 990600 DSC-cell) employing heating rates in the range 0.033 to 0.33 K sec^{-1}. In order to avoid anomalous heat effects due to cold work the pans were annealed and the ribbons were cut into fragments of length about 2 mm.

3. Results and discussion

3.1. Morphology

The wheel-side of ribbons, which were studied by SEM, showed a primary aluminium-rich solidification structure for alloys up to about 25 at% Si (Fig. 1a). At higher silicon contents a primary silicon-rich solidification structure was observed (Fig. 1b). In thin, electron-transparent parts of the ribbons, which were studied by TEM, this change in solidification structure was observed at about 30 at% Si. Thus an Al–Si-alloy which is hypereutectic under equilibrium conditions can have a hypoeutectic structure as a result of undercooling through rapid-quenching. This effect has been explained for eutectic metal-systems [8]. Depending on which phase grows fastest at a given undercooling, a structure develops which consists of either both primary and eutectic phases or eutectic phases only. In the aluminium–silicon system the primary aluminium-rich phase grows dendritically (Fig. 1a), whereas the silicon-rich phase grows in a faceted manner (Fig. 1b). The faceted phase is likely to grow more slowly at the occurring undercooling.

3.2. Metastable solid solubility

3.2.1. Lattice parameter results

3.2.1.1. Lattice parameter of the aluminium-rich phase as a function of composition. Literature data for the lattice parameter, a, of homogeneous f c c aluminium–silicon solid solutions, obtained by quenching from the solid state, are available up to 0.93 at% Si [9]. These data can be fitted to a linear relationship (compare with Fig. 2) such that

$$a_{294\,\mathrm{K}} = 0.40491 - 0.0174\,x_{\mathrm{Si}} \qquad (1)$$

where x_{Si} is the atomic fraction of silicon and a is given in nm. It is noted that Equation 1 differs appreciably from a linear interpolation (Vegard's law) between the lattice parameter of aluminium ($a = 0.40491$ nm) and of imaginary cubic close packed silicon ($a = 0.3731$ nm, as obtained from

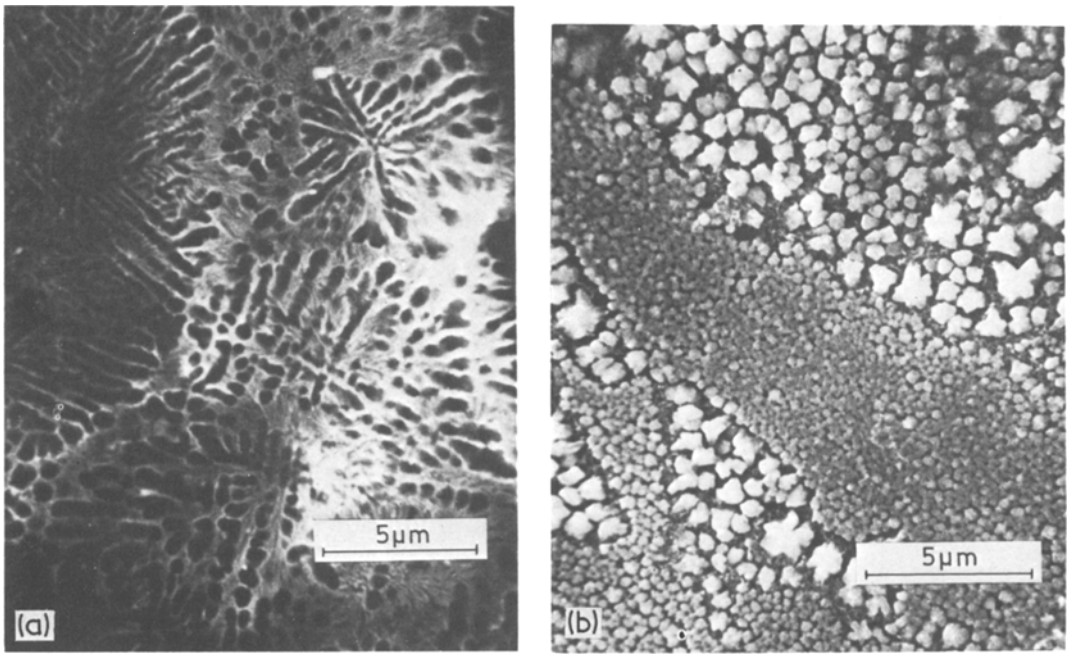

Figure 1 Solidification structure of Al–Si-alloys containing (a) 25 at% Si and (b) 33 at% Si, respectively, as observed by SEM.

the atomic radius after correction for cubic close packing [10]). Moreen, Taggart and Polonis [11] presented a model for the lattice parameter of a metallic solid solution as a function of composition and they showed that for a number of binary cubic solid solutions a parabolic curve fits very well with the experimental data. Application of their model to the Al–Si system gives (Fig. 2)

$$a_{294\mathrm{K}} = 0.40491 - 0.0174\,x_{\mathrm{Si}} - 0.0144\,x_{\mathrm{Si}}^2, \quad (2)$$

where a is given in nm.

The metastable silicon solid solubilities reported in [12] support the use of either Equation 1 or

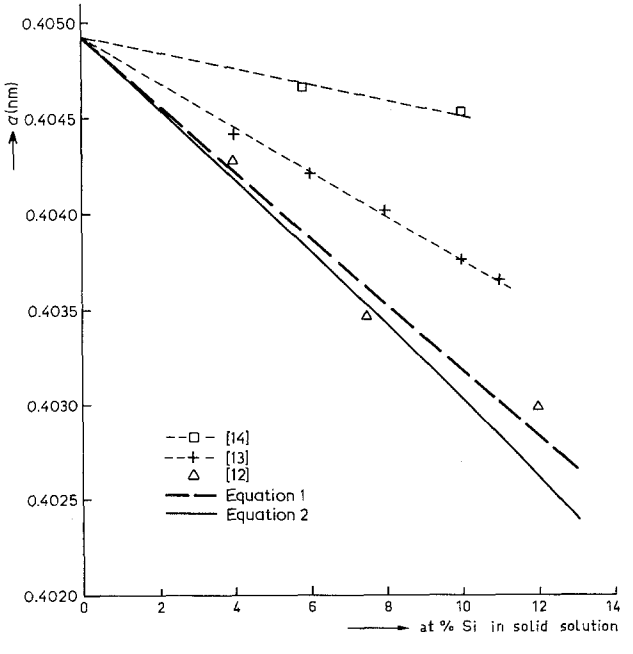

Figure 2 The lattice parameter a at 294 K of homogeneous Al–Si-alloys as a function of silicon content in solid solution. Data according to [12–14] are indicated. The solid line corresponds to Equation 2 and the dashed line corresponds to Equation 1.

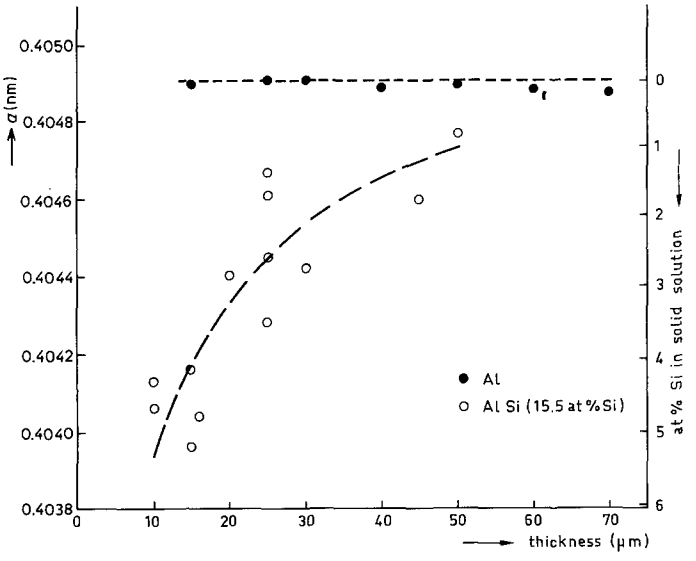

Figure 3 The lattice parameter a at 294 K, obtained from Debije–Scherrer photographs, and the silicon content in solid solution of the aluminium-rich phase in a melt-spun Al–Si-alloy with 15.5 at % Si and of melt-spun pure aluminium as a function of specimen thickness.

Equation 2. However, discrepancies exist with other work on rapidly quenched Al–Si-alloys [13, 14], where it was assumed that no silicon-rich phase was present in the specimens and thus the lattice parameter measured would correspond to an aluminium-rich phase with all the silicon in solid solution. Further, the results from the literature differ strongly (see Fig. 2). To explain these differences, it is suggested that very small silicon-rich particles are present which are hard to detect because they yield broad, weak lines on the diffractograms [13] or on the Debije–Scherrer photographs [14]. The failure to detect silicon-rich particles by TEM [13] does not exclude their presence since only very thin electron-transparent regions of the specimens, corresponding to the highest cooling rates, were investigated. From Fig. 2 it is seen that also the lattice parameter values reported in [13, 14] do not exclude the presence of a silicon-rich phase.

In this paper Equation 2 has been applied for the determination of metastable silicon solid solubilities.

3.2.1.2. Effects due to specimen thickness and alloy composition. It can be assumed that for a given rapid-quenching technique the thickness of the specimen obtained is indicative of the average cooling rate, provided that the experimental conditions are reasonably constant. The thinner a specimen is, the higher the cooling rate is and hence the larger the silicon content in solid solution, see Fig. 3.

For splat-cooled aluminium the lattice parameter was reported [15] to decrease with decreasing specimen thickness, an effect that was attributed to the presence of quenched-in excess vacancies. In the present study it was observed that the lattice parameter of melt-spun aluminium is independent of the specimen thickness within the range of thicknesses investigated (Fig. 3). It is concluded that the decrease of the lattice parameter of the melt-spun Al–Si-alloys is due to the increase of the silicon content in solid solution.

In Fig. 4 the metastable silicon solid solubility in the aluminium-rich phase is shown as a function

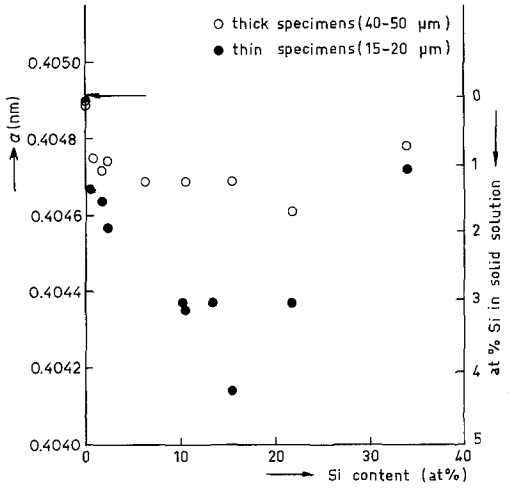

Figure 4 The lattice parameter a at 294 K of the aluminium-rich phase, obtained from Debije–Scherrer photographs, and the silicon content in solid solution as a function of alloy composition and specimen thickness. The lattice parameter of pure aluminium is indicated.

TABLE I Metastable silicon solid solubility in aluminium from lattice parameter measurements according to Equation 2. The corresponding lattice parameters are given in Fig. 2

Alloy composition (at % Si)	Specimen thickness (μm)	Solid solubility		Reference number
		Reported (at % Si)	Recalculated (at % Si)	
5.8	100–150	5.8	1.4	[14]
10.0	100–150	10.0	2.2	[14]
4.0	1–5	4.0	2.8	[13]
6.0	1–5	6.0	3.9	[13]
8.0	1–5	8.0	4.9	[13]
10.0	1–5	10.0	6.3	[13]
11.0	1–5	11.0	6.9	[13]

of alloy composition for two classes of specimen thicknesses: 15 μm to 20 μm and 40 μm to 50 μm. In Figs. 3 and 4 it is seen that there is a strong relation between specimen thickness and metastable solid solubility.

On the basis of Equation 2 the metastable solid solubilities reported by Itagaki *et al.* [13] and Bose and Kumar [14] have been recalculated (Table I). The revised values for the silicon solid solubilities of Bose and Kumar [14] are the smallest as they are obtained from rather thick specimens formed using a moderate cooling rate. After recalculation, the solid solubilities given in [13] are somewhat larger than those obtained in this study (see Table I). This can also be expected since the splat-cooling technique used by Itagaki, Giessen and Grant [13] gives a cooling rate higher (10^7 to 10^8 K sec^{-1}) than that obtained with the melt-spinning technique. Also, the specimen thickness reported (see Table I) may serve as an indication of these higher cooling rates.

From Fig. 4 it follows that the largest metastable silicon solid solubility in the aluminium-rich phase occurs at an alloy composition of about 15 at % silicon. This trend has been observed previously [12, 13]. This observation may be related to the finding [16] that silicon is present mainly as Si-clusters in molten hypereutectic alloys whilst in the hypoeutectic alloy silicon is present mainly as Al–Si-clusters.

The results presented in this section have been obtained from Debije–Scherrer photographs, which give information about a small region of a ribbon with a rather uniform thickness. In those instances where the lattice parameter is determined using a diffractometer, a large area is investigated and hence an average value for a greater range of thicknesses is obtained.

3.2.1.3. Lattice parameter of the silicon-rich phase. It was not possible to detect a dependence of the lattice parameter of the silicon-rich phase on specimen thickness by means of Debije–Scherrer photographs because the lines were very weak and broad. The lattice parameter as a function of alloy composition is best determined from diffractometer measurements, especially for low silicon contents; results are presented in Fig. 5. It follows that in the hypoeutectic alloys the silicon-rich phase has approximately the lattice parameter of pure silicon, whereas for the hypereutectic alloys the lattice parameter of the silicon-rich phase is considerably larger. (To our knowledge no lattice parameter data on the silicon-rich phase in rapidly quenched Al–Si-alloys have been reported before). The equilibrium solid solubility of aluminium in silicon is uncertain [1, 17]. Wamich [17] has reported lattice parameters of diluted solid solutions of aluminium in silicon. If the difference in

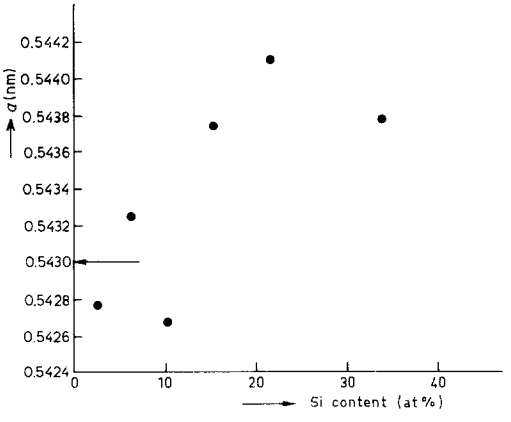

Figure 5 The lattice parameter *a* at 294 K of the silicon-rich phase, obtained from diffractometer measurements using the (3 1 1) reflection, as a function of alloy composition. The lattice parameter of pure silicon is indicated.

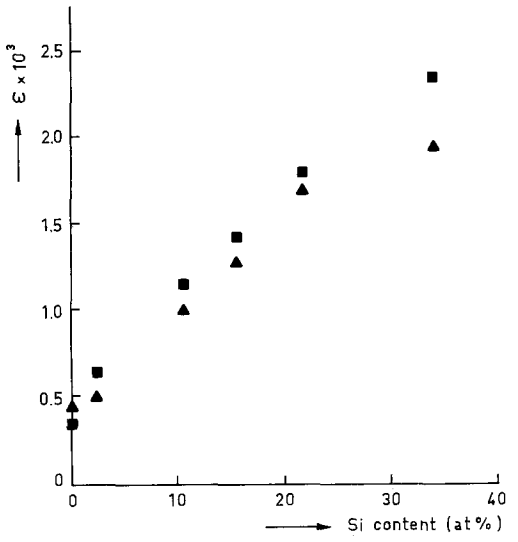

Figure 6 The microstrain ϵ in the ⟨111⟩- and ⟨100⟩-directions of the aluminium-rich phase as a function of alloy composition, shown by ▲ and ■, respectively.

lattice parameter of the silicon-rich phase in the hypereutectic alloy and pure silicon is interpreted as being due to aluminium in solid solution, an extrapolation of Wamich's data implies a metastable solid solubility of aluminium in silicon of about 7 at%.

3.2.2. Differential scanning calorimetry

Applying the sub-regular solution model, the metastable solid solubility of silicon in aluminium can be calculated from the experimentally determined enthalpy of precipitation [18]. Previously recorded thermodynamical data for the Al–Si-system in equilibrium are used [19, 20]. In addition it is assumed that no aluminium dissolves in the silicon-rich phase. According to the discussion in the previous section, this may imply that DSC should be restricted to hypoeutectic alloys.

In view of the relation between specimen thickness and metastable solid solubility (see Fig. 4) specimens for DSC should be prepared either from (i) a relatively large number of randomly selected pieces of ribbons or from (ii) a sufficiently large number of pieces of ribbons of approximately equal thickness. From specimens of the former type an average value for the silicon content in solid solution is obtained.

For an alloy with 10.2 at% Si, twelve specimens of type (i) gave values for the metastable solubility of silicon in aluminium that ranged between 1.2 at% and 2.0 at% Si, with an average value of 1.5 at% Si. For the same alloy, a specimen of type (ii) with pieces of ribbons thinner than 20 μm gave a solubility of 2.6 at% Si and specimen ribbons of about 90 μm in thickness gave a solid solubility of 0.5 at% Si. These results correspond to the lattice parameter results (Fig. 4). It is concluded that, although it is a laborious technique, DSC can give valuable results of metastable solid solubilities.

In addition, by changing the heating rate, the activation energy for the silicon precipitation is determined easily from the shift of the DSC peak maximum. For a melt-spun Al–Si-alloy with 10.2 at% Si an activation energy of 90 kJ mol^{-1} was found, which can be compared to values between 119 and 125 kJ mol^{-1} for precipitation in solid-quenched Al–Si-alloys [21]. Also in [22] a low activation energy in liquid-quenched material was reported, which was attributed to the presence of quenched-in excess vacancies.

3.3. Size-strain analysis

The crystallite sizes of, and the lattice distortions in, the aluminium-rich and silicon-rich phases can be determined by X-ray diffraction line profile analysis. A few line broadening studies of rapidly quenched metals and alloys have been performed [23–25], but not for the Al–Si-system.

In this paper, the pure, only structurally broadened, line profile is taken as the convolution of Cauchy and Gaussian profiles. The Cauchy and Gaussian profiles are identified with crystallite size and lattice-distortion broadening, respectively. In this way a single line profile suffices for the determination of size and strain effects (for details see [26]). The application of the single-line method in this investigation was justified because in tests results from (111) and (222) profiles, as well as from (200) and (400) profiles, coincided.

For the aluminium-rich phase, no crystallite size broadening was observed, implying a crystallite size larger than about 0.2 μm. This agrees with the theory developed in [27], from which grain sizes larger than 9 μm are predicted for cooling rates lower than 10^7 K sec^{-1}. The line broadening observed from the aluminium-rich phase is solely due to non-uniform lattice strains. The results are shown in Fig. 6. The lattice strain in the ⟨100⟩-direction is about 15% larger than in the ⟨111⟩-direction, which can be understood qualitatively since aluminium is softest in the ⟨100⟩-direction [28]. It is seen that there is a strong increase of the lattice strain with the silicon content of the

alloy. Considering that, in general, the major part of the silicon is present in a second phase, it is believed that the lattice strain in the aluminium-rich phase arises mainly from disturbances around the silicon-rich particles introduced during solidification. After solidification the two-phase alloy cooled down to room temperature resulting in an additional contribution to the line broadening as a result of the large difference between the thermal expansions of the silicon-rich and aluminium-rich phases [29, 30]. Further variations in the concentration of silicon in solid solution within the diffracting domains of the aluminium-rich phase, as well as differences in the average concentration of silicon in solid solution between the domains (noting that the fraction of silicon dissolved depends on the ribbon thickness, Figs. 3 and 4), may add to the line broadening observed [31, 32], thus leading to apparent strain values. The latter effect will be largest for the alloy containing 15.5 at% Si because that alloy exhibits the largest differences in silicon fraction dissolved (Fig. 4); the effect will be negligible for the alloy containing 33.9 at% Si, where the largest micro-strain is observed (Fig. 6).

Both size- and strain-broadening were found for the silicon-rich phase. The results of the (1 1 1), (2 2 0) and (3 1 1) profiles coincided. This implies that crystallite size and lattice strain are isotropic. The results are shown in Figs. 7 and 8. In conformity with these results, TEM studies indicated almost spherical particles with sizes of the same order of magnitude in alloys showing a hypoeutectic solidification structure. However, in the alloys with a hypereutectic solidification structure much larger particles were observed (Fig. 1b). X-ray diffraction analysis yielded small crystallite sizes for the hypereutectic alloys (Fig. 7) and, hence, the larger silicon-rich particles observed in the hypereutectic alloys consist of small, coherently diffracting domains. The smallest domain size of the silicon-rich phase is observed in alloys containing 15 at% Si.

3.4. Discussion of structural features accompanying the change in solidification behaviour

For alloys with a silicon content below 25 to 30 at% Si SEM and TEM studies showed structures characteristic of a hypoeutectic solidification, and for alloys with a higher silicon content structures typical of a hypereutectic solidification were revealed. Only regions with the highest cooling rates were investigated by both SEM and TEM methods.

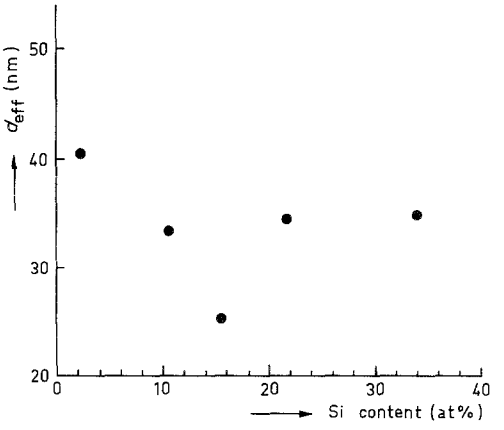

Figure 7 The effective crystallite size, d_{eff}, of the silicon-rich phase as a function of alloy composition.

X-ray diffraction gives information on the average structure of the ribbons. It was found that for an alloy composition of about 15 at% Si:

(a) the metastable solid solubility of silicon in aluminium is largest (Fig. 4),

(b) the lattice parameter of the silicon-rich phase changes abruptly (Fig. 5),

(c) the domain size of the silicon-rich phase is smallest (Fig. 7),

(d) the lattice strain in the silicon-rich phase changes abruptly (Fig. 8).

It may be concluded that, on average, the

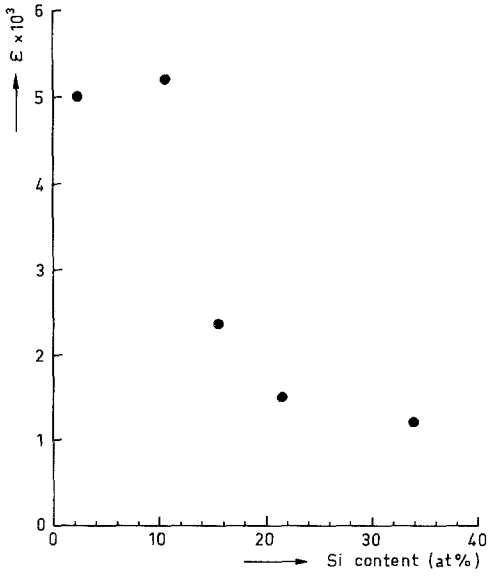

Figure 8 The microstrain ϵ in the silicon-rich phase as a function of alloy composition.

transition from hypoeutectic to hypereutectic solidification in melt-spun Al–Si-alloys occurs at about 15 at% Si.

Acknowledgement

The authors are indebted to Professor D. A. Granger for critically reading the manuscript.

References

1. L. F. MONDOLFO, "Aluminium Alloys, Structure and Properties" (Butterworths, London, 1976) p. 168.
2. J. R. BEDELL, Allied Chemical Corporation, U.S. Patent No. 3 862 658, 28 January 1975.
3. W. A. DEAN and R. E. SPEAR, Proceedings of the 12th Sagamore Army Materials Research Conference, Syracuse, New York, August 1965, edited by J. J. Burke, N. L. Reed and V. Weiss (Syracuse University Press, New York, 1966) p. 268.
4. H. MATYA, B. C. GIESSEN and N. J. GRANT, *J. Inst. Met.* **96** (1968) 30.
5. H. P. KLUG and L. E. ALEXANDER, "X-ray diffraction procedures" (John Wiley & Sons, New York, 1974) p. 594.
6. R. DELHEZ, Th. H. DE KEIJSER, E. J. MITTEMEIJER and N. M. VAN DER PERS, Proceedings of the Conference on Applied Crystallography, Kozubnik, Poland, August, 1978, Vol. I, edited by Z. Bojarksi and T. Bod (Silesian University, in Katowice and Institute of Ferrous Metallurgy in Gliwice, Katowice, Poland, 1979) p. 323.
7. R. DELHEZ and E. J. MITTEMEIJER, *J. Appl. Cryst.* 8 (1975) 609.
8. J. D. HUNT and K. A. JACKSON, *Trans. Met. Soc. AIME* **239** (1967) 864.
9. H. J. AXON and W. HUME-ROTHERY, *Proc. Roy. Soc.* **A193** (1948) 1.
10. W. B. PEARSON, "The Crystal Chemistry and Physics of Metals and Alloys" (Wiley Interscience, New York, 1972) p. 135.
11. H. A. MOREEN, R. TAGGART and D. H. POLONIS, *Met. Trans.* **2** (1971) 265.
12. P. H. SHINGU, K. KOBAYASHI, K. SHIMOMURA and R. OZAKI, *J. Jap. Inst. Met.* **37** (1973) 433.
13. M. ITAGAKI, B. C. GIESSEN and N. J. GRANT, *Trans. ASM* **61** (1968) 330.
14. S. K. BOSE and R. KUMAR, *J. Mater. Sci.* 8 (1973) 1795.
15. A. KIRIN, A. TONEJC and A. BONEFAČIĆ, *Scripta Met.* 3 (1969) 943.
16. M. SINGH and R. KUMAR, *J. Mater. Sci.* 8 (1973) 317.
17. F. WAMICH, PhD Thesis, Technical University of Aachen, West Germany, 1965.
18. A. BENDIJK, G. H. M. GUBBELS and L. KATGERMAN, unpublished work.
19. R. HULTGREN, P. D. DESAI, D. T. HAWKINS, M. GLEISER and K. K. KELLEY, "Selected Values of the Thermodynamic Properties of Binary Alloys" (American Society for Metals, Metals Park, Ohio, 1973) p. 210.
20. A. R. MIEDEMA, *J. Less Common Metals* **46** (1976) 67.
21. W. KÖSTER and W. KNORR, *Z. Metallk.* **45** (1954) 616.
22. H. MATYA, K. C. RUSSELL, B. C. GIESSEN and N. J. GRANT, *Met. Trans. A*, 6 (1975) 2249.
23. P. RAMACHANDRARAO and T. R. ANANTHARAMAN, *Trans. Met. Soc. AIME* **245** (1969) 892.
24. P. RAMACHANDRARAO, P. R. RAO and T. R. ANANTHARAMAN, *Z. Metallk.* **61** (1970) 471.
25. A. KIRIN and A. BONEFAČIĆ, *J. Phys. F.* 4 (1974) 1608.
26. Th. H. DE KEIJSER, J. I. LANGFORD, E. J. MITTEMEIJER and A. B. P. VOGELS, unpublished work.
27. P. G. BOSWELL and G. A. CHADWICK, *Scripta Met.* **11** (1977) 459.
28. C. J. SMITHELLS, "Metals Reference Books" 5th edn. (Butterworths, London, 1976) p. 978.
29. E. J. MITTEMEIJER, P. VAN MOURIK and Th. H. DE KEIJSER, *Phil. Mag.*, in press.
30. F. H. COCKS and S. F. COGAN, *J. Mater. Sci.* **11** (1976) 2061.
31. E. J. MITTEMEIJER and R. DELHEZ, *J. Appl. Phys.* **49** (1978) 3875.
32. *Idem*, Proceedings of the National Bureau of Standards Conference, Gaithersburg, Maryland, June 1979, NBS Special Publication 567, edited by S. Block and C. R. Hubbard (U.S. Department of Commerce, National Bureau of Standards, Washington, D.C., 1980) p. 271.

Received 13 March and accepted 2 April 1980.